3B İleri Biyobaskı Teknolojileri için Geçici Destek Malzemeleri Kullanılarak Baskılanmış Nöronal Sferoidler

Tuğrul Tolga DEMİRTAŞ 10

*1 Erciyes Üniversitesi Eczacılık Fakültesi, KAYSERİ

(Alınış / Received: 05.08.2025, Kabul / Accepted: 21.08.2025, Online Yayınlanma / Published Online: 30.08.2025)

Anahtar Kelimeler

3B biyobaskı, Nöronal sferoid, Destek (kurban) malzeme Öz: Nöral doku mühendisliğinde fizyolojik olarak ilgili 3B doku modellerinin geliştirilmesi önemli bir zorluk teşkil etmektedir. Bu çalışma, yapısal ve fonksiyonel özellikleri geliştirmek amacıyla SH-SY5Y sferoid yapılarının 3B biyobaskısında sodyum alJinat gibi geçici (kurban) malzemelerin kullanımını incelemektedir. Ortalama 80–100 µm çapında sferoidler oluşturulmuş ve canlı/ölü, Presto Blue ve immünsitokimyasal boyama teknikleriyle canlılık, çoğalma ve farklılaşma açısından değerlendirilmiştir. Sonuçlar, %90'ın üzerinde canlılık oranıyla başarılı sferoid oluşumunu, optimize edilmiş biyobaskı ile tutarlı filament desenlerini ve 14. günde çoğalma plato seviyesini göstermiştir. 14. günde konfokal mikroskop ile yapılan incelemeler, yoğun MAP2 ve TAU ekspresyonunu ortaya koymuş, bu da sağlam dendritik ve aksonsal gelişimi ve uzamış nörit ağlarını işaret etmiştir. Bu bulgular, kurban malzeme tabanlı biyobaskının, araştırma ve terapötik uygulamalar için 3B nöral doku modellerini ilerletme potansiyelini vurgulamaktadır.

Engineered Neuronal Spheroids Using Sacrificial Materials for 3D Advanced Bioprinting

Keywords

3D bioprinting, Neuronal spheroids, Sacrificial materials **Abstract:** The development of physiologically relevant 3D tissue models remains a challenge in neural tissue engineering. This study explores the use of sacrificial materials, such as sodium alginate, in the 3D bioprinting of SH-SY5Y spheroid constructs to enhance structural and functional properties. Spheroids with an average diameter of 80–100 µm were formed and assessed for viability, proliferation, and differentiation using Live/Dead, Presto Blue, and immunocytochemical staining techniques. Results indicated successful spheroid formation with over 90% viability, optimized bioprinting with consistent filament patterns, and a proliferation plateau by day 14. Confocal microscopy on day 14 revealed intense MAP2 and TAU expression, signifying robust dendritic and axonal development, alongside extended neurite networks. These findings underscore the potential of sacrificial material-based bioprinting to advance 3D neural tissue models for research and therapeutic applications.

1. Introduction

^{*}İlgili Yazar, email: ttolgad@erciyes.edu.tr

The printing of cell spheroids has emerged as a crucial component in tissue engineering and regenerative medicine, facilitating the creation of complex three-dimensional (3D) biological structures that mimic native tissues. Spheroids, as multicellular aggregates that exhibit enhanced cell-cell interactions, contribute significantly to achieving physiological relevance in tissue models due to their ability to recapitulate structural and functional properties akin to in vivo environments [1]. The intricate nature of bioprinting these structures involve the utilization of sacrificial materials, which serve as temporary scaffolds, allowing for the engineered spheroids to maintain their shape and positioning during the printing process and subsequent culture [2].

Sacrificial materials, often hydrogels or soluble polymers, play a crucial role in ensuring the mechanical fidelity of printed constructs. Various biodegradable and biocompatible compounds are often highlighted as suitable for this purpose. Sodium alginate (NaAlg), a natural polysaccharide, is frequently employed due to its low toxicity, gentle crosslinking processes, and favorable environmental profile. It offers an ideal environment for the encapsulation of cells while maintaining shape integrity during the early phases of printing [3]. Other commonly used materials include Pluronic F-127 and gelatin, which enhance the printability and support the structural properties of the bioprinted constructs [4, 5]. These materials are typically integrated into complex multi-component bioinks to achieve the desired viscosity and printability.

Several studies have demonstrated approaches to effectively print cell spheroids using sacrificial strategies, showing that the choice of material significantly impacts the efficacy of the printing process. For instance, Kim et al. explored freeform bioprinting techniques using alginate microgels as a supporting medium, illustrating how such methods improve the physiological relevance of constructed tissues due to a more favorable microenvironment [6]. Similarly, Jin et al. adopted a printing-then-casting method, utilizing a fugitive pattern with alginate, which allowed the fabrication of vascular network scaffolds [3]. The strategic cross-linking and subsequent dissolution of sacrificial materials enable the generation of architectures that closely resemble natural vasculature, essential for nutrient transport within larger tissues.

Moreover, advances in bioprinting technologies have facilitated the incorporation of multiple cell types and the creation of composite spheroids that support dynamic interactions among different cell populations. For example, Zhang et al. emphasized the importance of layering different cell types within spheroids to generate functional models, suggesting that a microfluidic approach allows for precise control over spheroid synthesis due to the timed delivery of cells [7, 8]. The ability to customize printing parameters and bioink compositions leads to spheroids that not only retain viability post-printing but also provide a conducive environment for tissue maturation and function [9].

On the computational front, studies such as that by Robu et al. have employed simulations to model the behavior of cell spheroids under various bioprinting conditions. These computational models guide the design of functional vascular networks, substantially impacting their efficacy in drug delivery systems and engineered organ constructs [10, 11]. Furthermore, research continues to evolve with innovations like self-assembling methodologies that eliminate the need for traditional sacrificial supports, thereby enhancing cell viability and integration [12].

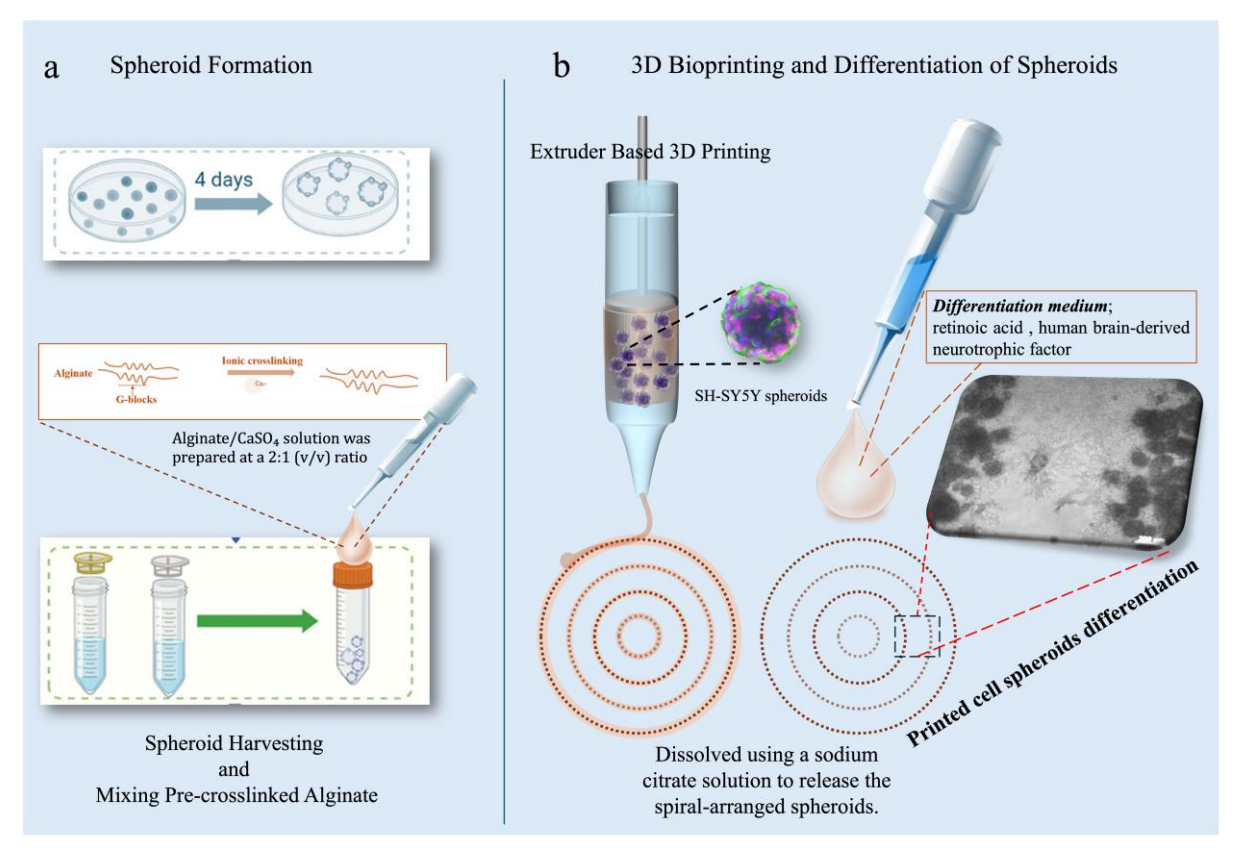
Consequently, despite advances in 3D bioprinting, the development of stable, functional neuronal spheroid constructs remains a critical challenge, particularly in maintaining structural integrity and promoting long-term differentiation. The successful formation of SH-SY5Y spheroids with diameters of $80\text{--}100~\mu m$ and viability exceeding 90% highlights the potential of sacrificial materials like sodium alginate to overcome initial printing hurdles. However, the observed plateau in proliferation by day 14, coupled with the emergence of network-like structures, suggests a transition toward cellular maturation. Furthermore, the robust expression of MAP2 and TAU on day 14, indicative of advanced dendritic and axonal development, underscores the feasibility of achieving physiologically relevant neuronal models. This study seeks to explore the factors influencing this maturation process and optimize culture conditions to enhance the functional outcomes of 3D-printed neuronal spheroids, paying the way for their application in neurobiological research and regenerative medicine.

2. Material and Method

2.1. Cell culture

SH-SY5Y human neuroblastoma cells (ATCC, CRL-2266) were maintained in Dulbecco's Modified Eagle Medium/Nutrient Mixture F-12 (DMEM/F12, Thermo Fisher Scientific) supplemented with 10% fetal bovine

serum (FBS, Thermo Fisher Scientific) and 1% penicillin-streptomycin (100 U/mL penicillin, 100 μ g/mL streptomycin, Thermo Fisher Scientific). Cells were cultured at 37°C in a humidified incubator with 5% CO₂. The



culture medium was replaced every 2–3 days, and cells were passaged at 80–90% confluency using 0.25% trypsin-EDTA (Thermo Fisher Scientific). Cells between passages 5 and 15 were used for experiments.

Figure 1. Schematic illustration of SH-SY5Y cell spheroid formation and bioprinting. (a) Spheroid formation process using ultra-low attachment plates. (b) 3D bioprinting and differentiation of spheroids into spiral constructs.

2.2. Spheroid formation

For spheroid formation, SH-SY5Y cells were harvested from monolayer cultures and resuspended in DMEM/F12 supplemented with 10% FBS and 1% penicillin-streptomycin. Cells were seeded at a density of 5×10^4 cells/well in 24-well ultra-low attachment plates (Corning, CLS3474). Plates were centrifuged at $200 \times g$ for 5 minutes to promote cell aggregation. Spheroids were cultured at 37° C in a humidified incubator with 5% CO₂ for 4 days, with the medium refreshed every 2 days (Figure 1a). Spheroid formation was confirmed by visual inspection under a light microscope, with spheroids reaching an average diameter of $80-100~\mu m$.

2.2.1. Cell viability assessment of spheroids (Live and dead assay)

The viability of SH-SY5Y cell spheroids was evaluated using a Live/Dead Viability/Cytotoxicity Kit (Thermo Fisher Scientific). Prior to staining, the cell-laden hydrogels were rinsed twice with phosphate-buffered saline (PBS) to remove residual media. The samples were then incubated in a staining solution containing 2 μ M Calcein AM and 4 μ M Ethidium Homodimer-1 (EthD-1) for 30 minutes at 37°C in a dark environment. Following incubation, the samples were visualized using a Zeiss LSM 510 confocal microscope (Germany) equipped with appropriate excitation and emission filters (488 nm for Calcein AM and 561 nm for EthD-1). Quantitative analysis of microscopy data was performed using ImageJ software, where fluorescence intensity and live/dead cell ratios were determined through automated thresholding and region-of-interest selection.

2.3. Bioprinting optimization and printing of cell spheroid-laden hydrogels

Sodium alginate (Sigma-Aldrich) was dissolved in phosphate-buffered saline (PBS, pH 7.4, 0.01 M phosphate, 0.137 M NaCl) at a concentration of 3% (w/v) under constant stirring at room temperature for 2 hours to ensure complete dissolution. Calcium sulfate (CaSO₄, Sigma-Aldrich) was then added to the sodium alginate solution at a concentration of 1% (w/v) to initiate internal gelation, as described by [13]. The mixture was gently agitated for 15 minutes at room temperature to facilitate uniform crosslinking, resulting in a stable gel matrix.

Subsequently, the alginate/ $CaSO_4$ solution was prepared at a 2:1 (v/v) ratio by combining the pre-crosslinked alginate solution with a $CaSO_4$ solution. This mixture was thoroughly mixed 300 times using a three-way tap.

SH-SY5Y cell spheroids, formed as described in the Spheroid Formation section, were gently mixed into the precrosslinked 3% alginate (w/v) solution at a ratio of approximately 1000 spheroids per mL with a three-way tap. The mixture was kept at 4° C to maintain spheroid viability and prevent premature gelation prior to printing.

Bioprinting was conducted using a custom 3D bioprinter with a 22-gauge nozzle on poly-L-lysine-coated coverslips. The pre-crosslinked alginate solution containing SH-SY5Y spheroids was loaded into the printing cartridge. A spiral geometry was chosen for the bioprinted constructs to promote uniform spheroid distribution, enhance nutrient and oxygen diffusion through the curved architecture, and mimic the interconnected network-like structures of neural tissues [3]. This design facilitates cellular interactions and supports the formation of complex tissue architectures, as demonstrated in studies utilizing curved scaffolds for tissue engineering [3]. Optimization of filament length and height was performed by varying printing pressures (2, 4, 6, 8, and 10 psi) and deposition speeds (5, 15, 25, 35, 45, and 55 mm/s), resulting in consistent filament structures. The alginate acted as a sacrificial material, providing temporary support during printing, and was subsequently dissolved using a 50 mM sodium citrate solution to release the spiral-arranged spheroids (Figure 1b). Filament dimensions and spiral characteristics (e.g., turn diameter and spheroid distribution) were evaluated post-printing using light microscopy.

2.4. Printed cell spheroid differentiation

For neuronal differentiation, after alginate removal, the printed spiral-arranged SH-SY5Y spheroids were cultured in DMEM/F12 supplemented with 10% FBS and 1% penicillin-streptomycin at 37°C in a humidified incubator with 5% CO_2 . After 24 hours, the medium was replaced with DMEM/F12 containing 1% FBS and 10 μ M all-transretinoic acid (RA, Sigma-Aldrich, dissolved in DMSO). The RA-containing medium was renewed every 2 days for 5 days [14]. Subsequently, cells were switched to serum-free DMEM/F12 supplemented with 50 ng/mL recombinant human brain-derived neurotrophic factor (BDNF, PeproTech, 450-02, reconstituted in sterile water) and 1% penicillin-streptomycin. The BDNF-containing medium was renewed every 2 days for an additional 3 days [15]. Differentiated cells exhibited neuronal morphology, characterized by extended neurites, and were used for subsequent experiments (Figure 1b).

2.4.1. Cell proliferation analysis for printed spheroids (Presto Blue assay)

Cell proliferation of 3D-printed SH-SY5Y spheroids was assessed using the Presto Blue Cell Viability Reagent (Thermo Fisher Scientific) on days 2, 3, 8, and 13 following the bioprinting process. For each analysis, the culture medium was aspirated and replaced with a working solution consisting of 10% (v/v) Presto Blue reagent diluted in fresh DMEM/F12 supplemented with 10% FBS and 1% penicillin-streptomycin. The printed spheroids were incubated with the reagent for 2 hours at 37° C in a humidified atmosphere with 5% CO₂, protected from light to preserve fluorescence. Following incubation, fluorescence intensity was measured using a fluorescence microplate reader at an excitation wavelength of 560 nm and an emission wavelength of 590 nm. Measurements were recorded for three technical replicates per time point, with background fluorescence corrected using a blank consisting of medium with reagent alone, to evaluate proliferation trends over the culture period.

2.4.2 Immunocytochemistry staining

Immunocytochemical staining was performed on differentiated SH-SY5Y cells to assess neuronal marker expression. Cells, cultured on poly-L-lysine-coated coverslips following a 14-day differentiation protocol with all-trans-retinoic acid and brain-derived neurotrophic factor, were fixed with 4% paraformaldehyde in phosphate-buffered saline (PBS) for 15 minutes at room temperature. Subsequently, cells were permeabilized with 0.1% Triton X-100 in PBS for 10 minutes and blocked with 5% bovine serum albumin (BSA) in PBS for 1 hour to reduce non-specific binding. Primary antibodies, including mouse anti-MAP2 (1:500, Abcam) and rabbit anti-TAU (1:500, Thermo Fisher Scientific), were applied overnight at 4°C. After washing with PBS, secondary antibodies, Alexa Fluor 594-conjugated goat anti-mouse (1:1000, Invitrogen) for MAP2 and Alexa Fluor 488-conjugated goat anti-rabbit (1:1000, Invitrogen) for TAU, were incubated for 1 hour at room temperature in the dark. Nuclei were counterstained with 4',6-diamidino-2-phenylindole (DAPI, 1 μ g/mL) for 5 minutes. Samples were mounted using a fluorescence-preserving medium (ProLong Gold, Thermo Fisher Scientific) and visualized using a Zeiss LSM 510 confocal microscope (Germany) with excitation wavelengths of 405 nm (DAPI), 488 nm (TAU), and 561 nm (MAP2). Z-stack images were acquired at 1 μ m intervals to capture the three-dimensional distribution of staining.

3. Results

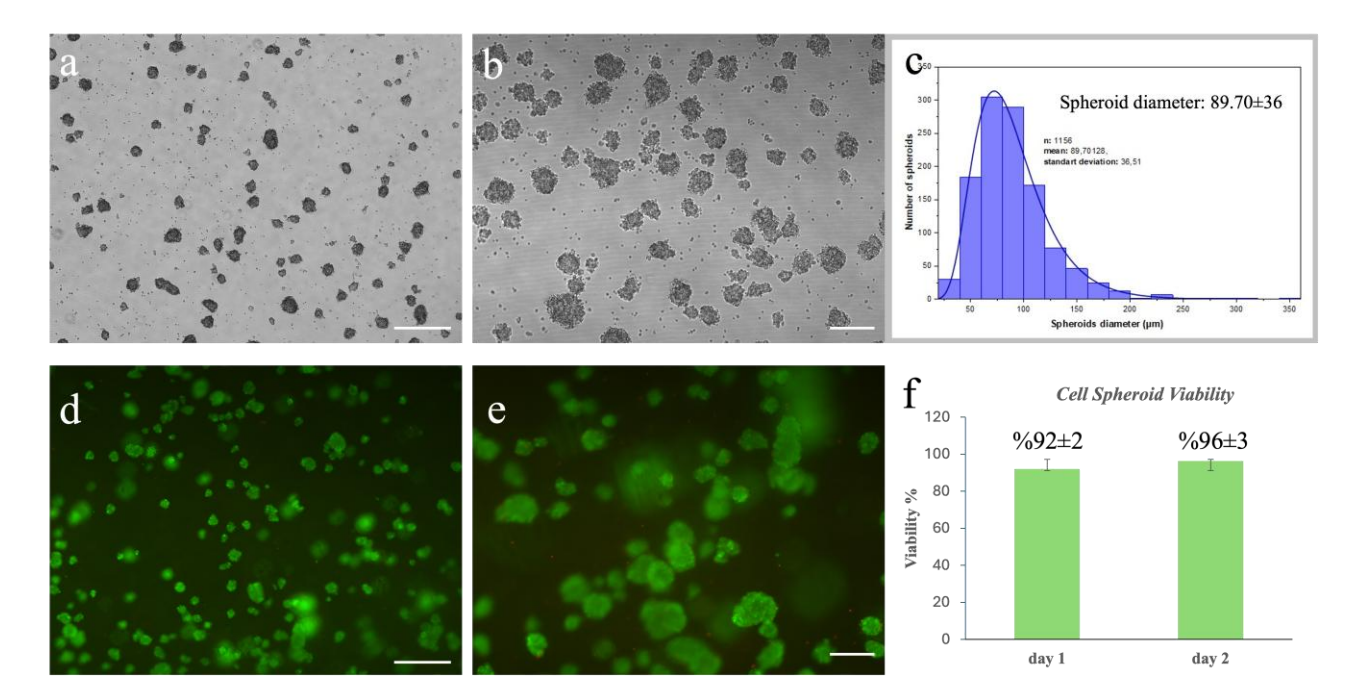


Figure 2. Morphological and quantitative evaluation of SH-SY5Y spheroids with random distribution. (a) Light microscope image of randomly arranged spheroid aggregates at 2.5x magnification. (b) Light microscope image of individual spheroid structures at 5x magnification. (c) Bar graph displaying average spheroid size (mean \pm SD) across experimental conditions, analyzed using ImageJ software. (d) Light microscope image of randomly distributed spheroids post-culture, stained with Live/Dead assay to assess viability, at 2.5x magnification. (e) Light microscope image of spheroid viability, highlighting live (green) and dead (red) cells via Live/Dead assay, at 5x magnification. (f) Bar graph illustrating spheroid cell viability (mean \pm SD) over time. Scale bars: 500 µm (a, d), 200 µm (b, e).

Figure 2 demonstrated successful spheroid formation of SH-SY5Y cells, as evidenced by the uniform aggregates observed in light microscope images. The average spheroid diameter, a critical parameter for 3D printing, was determined to be 89.70 ± 36 µm, with a range of approximately 53.70 to 125.70 µm, as depicted in Figure 2c. This size, while reflective of effective cell aggregation, falls slightly below the commonly reported optimal range of 100-200 µm for spheroid bioprinting, indicating potential challenges in maintaining structural stability and printing precision. However, viability assessment via the Live/Dead assay revealed a high proportion of living cells, with

green fluorescence predominating in Figures 2d and 2e, and quantitative analysis in Figure 2f confirming viability exceeding 90%, suggesting the spheroids' resilience despite their smaller diameter.

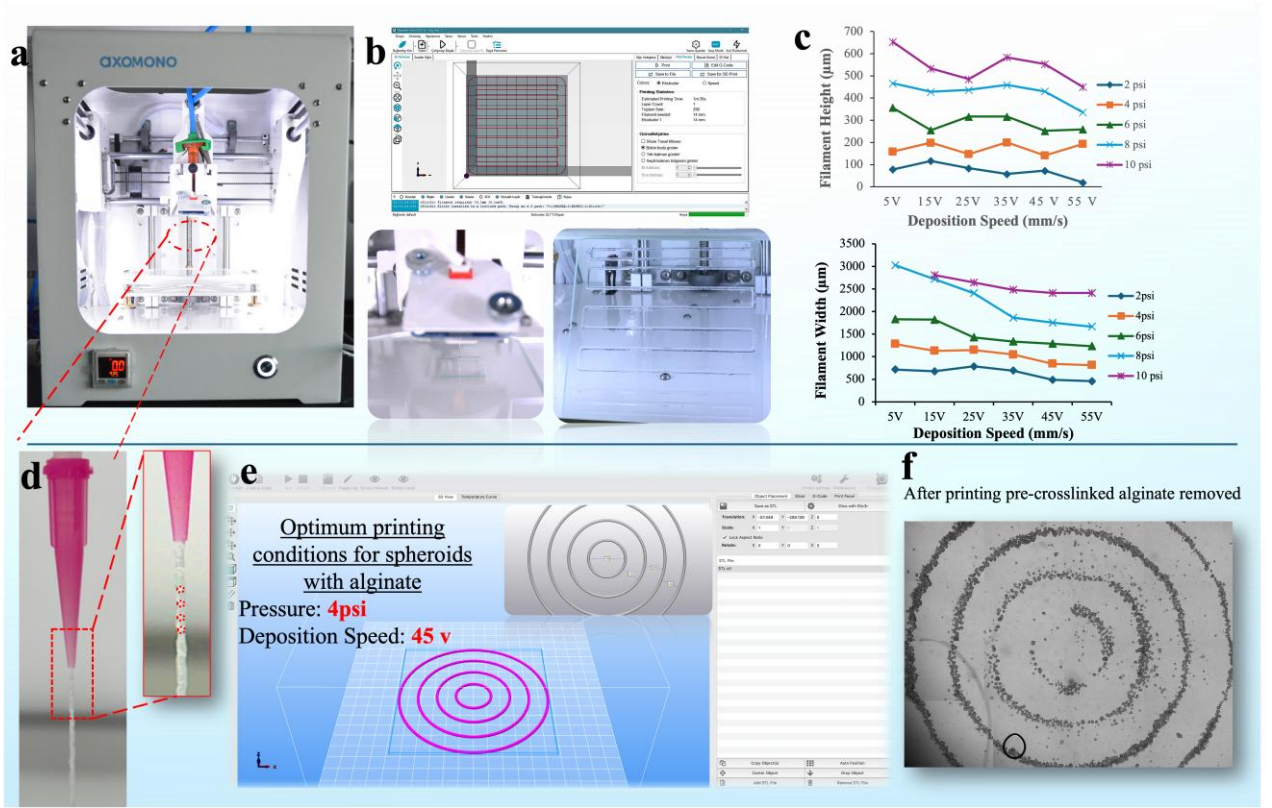


Figure 3. Bioprinting process and characterization of SH-SY5Y spheroid constructs. (a) Axolot extruder-based bioprinter utilized for spheroid printing. (b) Optimization process of 3% alginate with $CaSO_4$ using a zigzag model to assess printing parameters. (c) Graph depicting filament height and width as a function of deposition speed (5–55 mm/s) with spheroids embedded in alginate, measured via microscopy. (d) Photographic image of alginate flow from a gauge, showing spheroid distribution during extrusion. (e) 3D model of a spiral structure designed for bioprinting. (f) Light microscope image of printed spheroids after alginate removal, demonstrating structural integrity post-culture. Scale bars: 500 μm (f).

Figure 3a illustrated the efficacy of the axoloth extruder-based bioprinter, supporting the successful deposition of spheroid-laden alginate. Figure 3b demonstrated effective optimization of 3% alginate with $CaSO_4$ using a zigzag model, resulting in consistent filament patterns across tested conditions. In Figure 3c, filament height and width varied with deposition speed, with data indicating a decrease in height from 300 μ m to 150 μ m as speed increased from 5 to 55 mm/s, reflecting adaptability to spheroid incorporation. Figure 3d revealed uniform flow from the gauge, with spheroids clearly visible and intact during extrusion, suggesting robust material handling. Figure 3e presented a 3D model of a spiral structure, which served as the design template, while Figure 3f displayed printed spheroids after alginate removal, exhibiting well-defined structures that closely approximated the modeled spiral architecture.

Figure 4 revealed the temporal evolution of 3D-printed SH-SY5Y spheroid constructs from day 2 to day 14, with 4x4 mosaic images at 2.5x magnification (Figure 4a, 4d, 4g, 4j) displaying the whole spiral structure and paired images at 2.5x and 5x magnifications (Figure 4b, 4c, 4e, 4f, 4h, 4i, 4k, 4l) highlighting cellular details. At day 2, spheroids exhibited a defined spiral architecture with limited cellular extension. As days increased, notable changes emerged, with spiral layer cells beginning to spread and connect between day 7 and day 10, as observed in the 5x magnification images. By day 14, these connections matured into a network-like structure, evident in Figure 4i and 4l, indicating enhanced intercellular integration and structural complexity over the culture period.

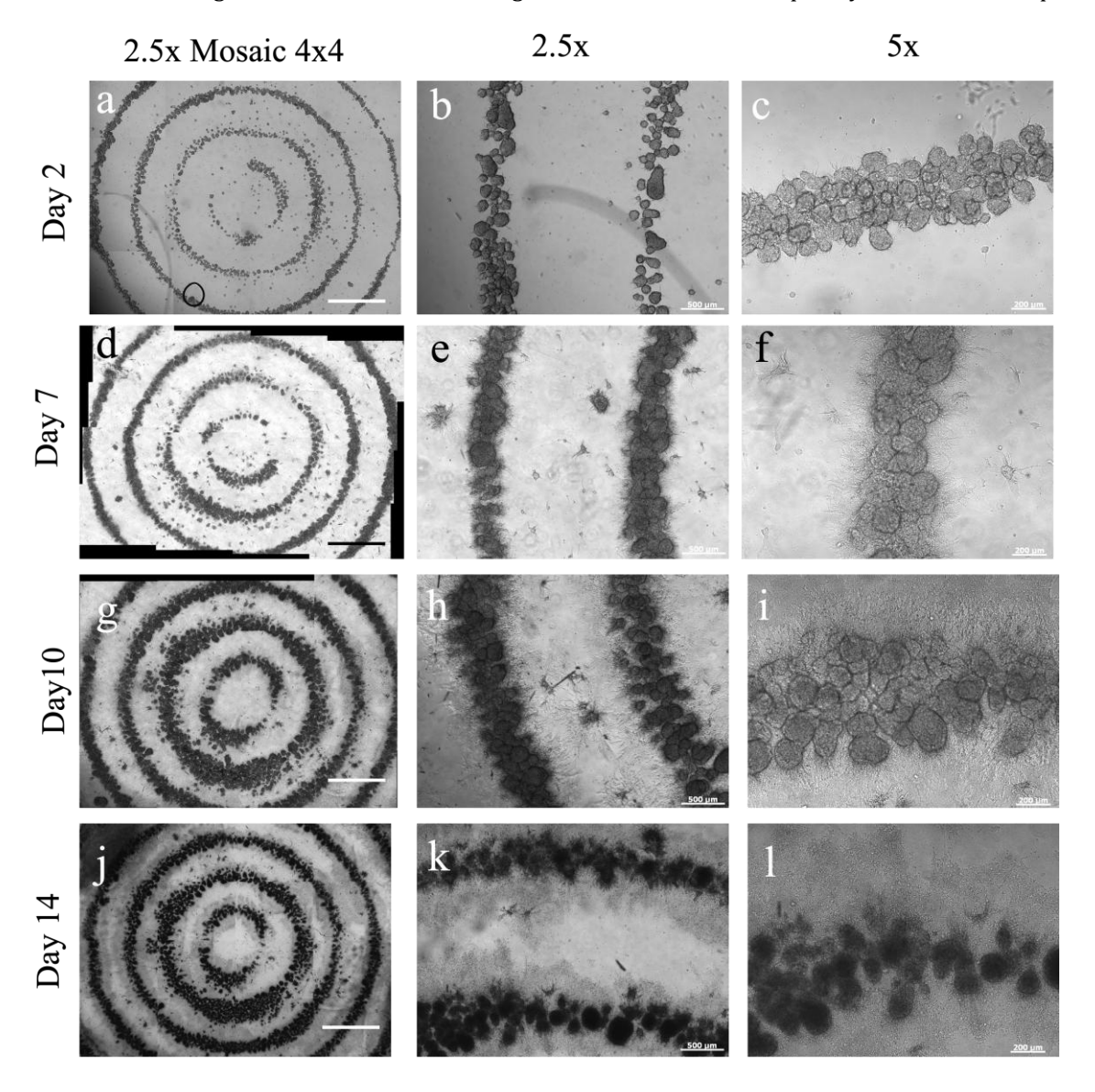


Figure 4. Temporal assessment of 3D-printed SH-SY5Y spheroid constructs across multiple magnifications. (a, d, g, j) 4x4 mosaic light microscope images at 2.5x magnification showing the entire printed structure on days 2, 7, 10, and 14, respectively. (b, e, h, k) Light microscope images at 2.5x magnification of printed spheroids on days 2, 7, 10, and 14, respectively. (c, f, i, l) Light microscope images at 5x magnification of printed spheroids on days 2, 2x

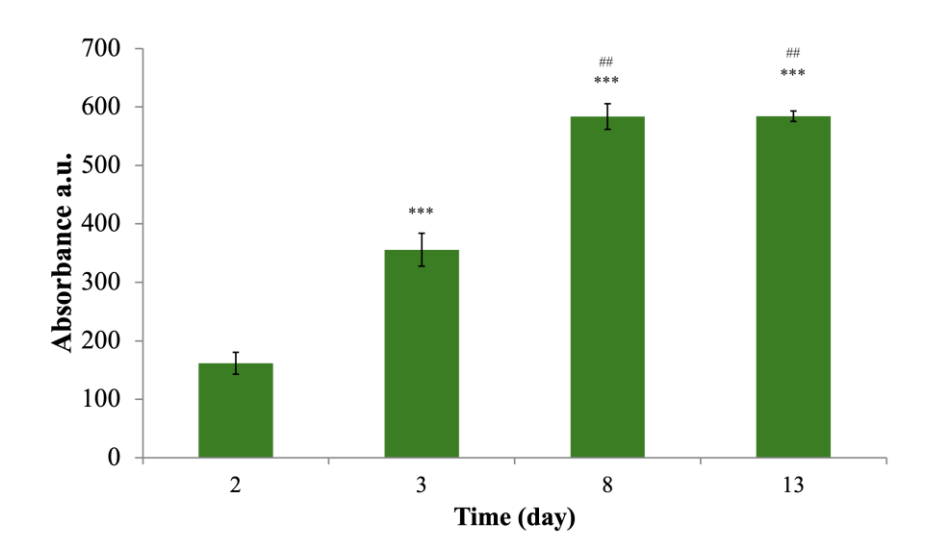


Figure 5. Presto Blue assessment of cell proliferation in 3D-printed SH-SY5Y spheroids across time intervals. Bar graph displaying mean fluorescence intensity (mean \pm SD) on days 2, 3, 8, and 13 post-printing, evaluated using the bar. Statistically significant differences: n = 3, *** p < 0.001 when the control group is day 2, ## p < 0.01 when the control group is day 3.

Cell proliferation in the 3D-printed SH-SY5Y spheroids was evaluated using the Presto Blue assay at days 2, 3, 8, and 13 post-printing (Figure 5). Metabolic activity showed a significant increase from day 2 to day 3 (***p < 0.001 vs. day 2), with further significant rises to day 8 (***p < 0.001 vs. day 2; ##p < 0.01 vs. day 3) and day 13 (***p < 0.001 vs. day 2; ##p < 0.01 vs. day 3). No significant difference was observed between day 8 and day 13 (one-way ANOVA followed by Tukey's HSD post-hoc test; n=3 replicates per time point).

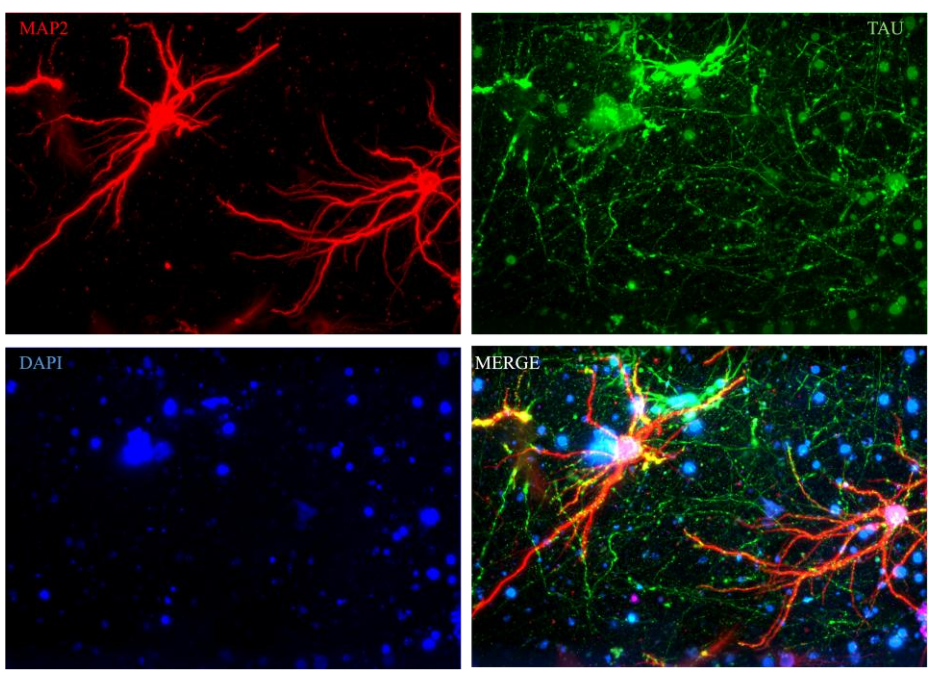


Figure 6. Confocal microscopy images of SH-SY5Y cell differentiation on day 14. (A) Immunofluorescence staining for MAP2 (red) highlighting neuronal dendrites. (B) Immunofluorescence staining for TAU (green) indicating

axonal structures. (C) DAPI staining (blue) showing cell nuclei. (D) Merged image of MAP2, TAU, and DAPI, demonstrating colocalization and extended neurite networks. Cells were differentiated using a sequential protocol with all-trans-retinoic acid and brain-derived neurotrophic factor, as described in the Materials and Methods. Scale bar, 50 µm.

Figure 6 demonstrated the differentiation of 3D-printed SH-SY5Y spheroids on day 14, as visualized through confocal microscopy. Immunofluorescence staining for MAP2, a microtubule-associated protein enriched in neuronal dendrites, revealed intense red fluorescence, indicating robust dendritic development and neuronal maturity. Staining for TAU, a microtubule-associated protein predominant in axons, exhibited prominent green fluorescence, signifying extensive axonal structures and suggesting healthy neuronal polarity and elongation. DAPI staining displayed blue fluorescence, marking cell nuclei and revealing a uniform distribution of cells within the constructs. The merged image highlighted colocalization of MAP2, TAU, and DAPI, with extended neurite networks evident, demonstrating successful integration and connectivity of differentiated neurons following the applied differentiation protocol.

4. Discussion and Conclusion

The 3D bioprinting of SH-SY5Y spheroids using sodium alginate as a sacrificial material achieved high viability (>90%) despite a smaller-than-optimal diameter of $89.70 \pm 36 \, \mu m$, compared to the commonly cited $100-200 \, \mu m$ range for optimal cellular aggregation and nutrient diffusion [16]. The high surface area-to-volume ratio of smaller spheroids likely enhanced nutrient exchange, mitigating structural stability challenges during printing [17, 18, 20]. Zhao et al. (2019) emphasized that optimized bioinks, such as the 3% alginate with calcium sulfate used here, maintain cell viability by reducing shear stress, supporting our findings [19]. Additionally, smaller spheroids offer a uniform environment for studying cellular responses, though they may lack the complexity of larger spheroids [21]. Moldovan et al. (2017) noted that spheroids with suboptimal sizes can still contribute to functional tissue constructs due to their self-assembling properties, aligning with our successful construct formation [22].

The bioprinting process demonstrated robust material handling and adaptability, with consistent filament patterns achieved using 3% alginate with $CaSO_4$ [23, 24, 25]. Filament height decreased from 300 μ m to 150 μ m as deposition speed increased (5–55 mm/s), indicating flexibility in achieving precise geometries [26, 27]. The uniform flow of spheroid-laden alginate during extrusion ensured structural integrity and cell viability, critical for multilayered constructs [28, 29]. The spiral architecture, which closely matched the designed 3D model, facilitated uniform spheroid distribution and mimicked neural tissue networks, enhancing biological responses and integration [30]. This design choice, inspired by studies like Jin et al. (2018), supports the development of complex tissue architectures [3].

Over the culture period, the spheroid constructs evolved from a defined spiral structure on day 2 to a mature network-like architecture by day 14, reflecting increased cellular connectivity [31, 32]. The Presto Blue assay showed significant proliferation from day 2 to day 3 (p<0.001) and day 3 to day 8 (p<0.001), followed by a plateau through day 13 (p>0.05, Tukey's HSD), suggesting a shift toward differentiation [36]. This aligns with Liu et al. (2019), who noted that nutrient limitations may drive such transitions in 3D neuronal cultures [36]. By day 14, robust MAP2 and TAU expression indicated advanced dendritic and axonal development, supporting neuronal polarity and connectivity [37, 38, 39, 40]. Desai et al. (2017) highlighted that interconnected networks are essential for mimicking physiological conditions, reinforcing the potential of these constructs for neural tissue engineering [34]. However, challenges with spheroid size and nutrient availability suggest opportunities for optimizing bioinks or incorporating vascular-like structures [3, 33, 35].

In conclusion, this study demonstrates that SH-SY5Y spheroids with a diameter of $89.70 \pm 36 \,\mu m$, though smaller than the optimal $100\text{--}200 \,\mu m$ range, achieve high viability (>90%) and robust neuronal differentiation when bioprinted with sodium alginate. The optimized bioink and spiral architecture enabled precise deposition and the formation of network-like structures by day 14, marked by significant MAP2 and TAU expression. These findings highlight the potential of sacrificial material-based bioprinting for neural tissue engineering, despite challenges with spheroid size. Future research should focus on enhancing bioink formulations and culture conditions to improve structural stability and nutrient delivery. Additionally, integrating advanced techniques, such as cold atmospheric plasma (CAP), could enhance biocompatibility and crosslinking efficiency of alginate while promoting neurogenic differentiation through surface modification [19, 20]. This synergy could advance the development of physiologically relevant 3D neural tissue models for research and therapeutic applications.

Acknowledgment

I thank AyşeNur Karadeniz for her contributions to ImageJ calculations and Burak Çevlik for his support in developing 3D STL models, both essential to this study.

References

- [1] Chae, S., Lee, H., Ryu, D., & Kim, G. 2024. Macroscale pseudo-spheroids fabricated using methacrylated collagen-coated cells. Theranostics, 14(3), 924-939. https://doi.org/10.7150/thno.92193
- [2] Liu, S., Wang, T., Li, S., & Wang, X. 2022. Application status of sacrificial biomaterials in 3d bioprinting. Polymers, 14(11), 2182. https://doi.org/10.3390/polym14112182.
- [3] Jin, Y., Chai, W., & Huang, Y. 2018. Fabrication of stand-alone cell-laden collagen vascular network scaffolds using fugitive pattern-based printing-then-casting approach. Acs Applied Materials & Interfaces, 10(34), 28361-28371. https://doi.org/10.1021/acsami.8b09177.
- [4] Lewis, P., Yan, M., Su, J., & Shah, R. 2019. Directing the growth and alignment of biliary epithelium within extracellular matrix hydrogels. Acta Biomaterialia, 85, 84-93. https://doi.org/10.1016/j.actbio.2018.12.039.
- [5] Kim, M., Jeong, W., Jeon, S., & Kang, H. 2023. 3d bioprinting of decm-incorporated hepatocyte spheroid for simultaneous promotion of cell-cell and -ecm interactions. Frontiers in Bioengineering and Biotechnology, 11. https://doi.org/10.3389/fbioe.2023.1305023.
- [6] Wang, C. and Zhou, Y. 2023. Sacrificial biomaterials in 3d fabrication of scaffolds for tissue engineering applications. Journal of Biomedical Materials Research Part B Applied Biomaterials, 112(1). https://doi.org/10.1002/jbm.b.35312.
- [7] Kim, M., Banerjee, D., Celik, N., & Özbolat, İ. 2022. Aspiration-assisted freeform bioprinting of mesenchymal stem cell spheroids within alginate microgels. Biofabrication, 14(2), 024103. https://doi.org/10.1088/1758-5090/ac4dd8c
- [8] Zhang, P., Li, X., Chen, J., & Abate, A. 2022. Controlled fabrication of functional liver spheroids with microfluidic flow cytometric printing. Biofabrication, 14(4), 045011. https://doi.org/10.1088/1758-5090/ac8622.
- [9] Nothdurfter, D., Ploner, C., Coraça-Huber, D., Wilflingseder, D., Müller, T., Hermann, M., ... & Ausserlechner, M. 2022. 3d bioprinted, vascularized neuroblastoma tumor environment in fluidic chip devices for precision medicine drug testing. Biofabrication, 14(3), 035002. https://doi.org/10.1088/1758-5090/ac5fb7.
- [10] Minaeva, E., Antoshin, A., Kosheleva, N., Koteneva, P., Гончуков, С., Tsypina, S., ... & Минаев, H. (2023). Laser bioprinting with cell spheroids: accurate and gentle. Micromachines, 14(6), 1152. https://doi.org/10.3390/mi14061152.
- [11] Robu, A., Mironov, V., & Neagu, A. (2019). Using sacrificial cell spheroids for the bioprinting of perfusable 3d tissue and organ constructs: a computational study. Computational and Mathematical Methods in Medicine, 2019, 1-9. https://doi.org/10.1155/2019/7853586.
- [12] Shi, J., Wan, Y., Jia, H., Skeldon, G., Cornelissen, D., Wesencraft, K., ... & Shu, W. (2024). Printing cell embedded sacrificial strategy for microvasculature using degradable dna biolubricant. Angewandte Chemie, 64(12). https://doi.org/10.1002/anie.202417510.
- [13] Demirtaş, T. T., Irmak, G., & Gümüşderelíoğlu, M. 2017. A bioprintable form of chitosan hydrogel for bone tissue engineering. Biofabrication, 9(3), 035003. https://doi.org/10.1088/1758-5090/aa7b1d.
- [14] Yamaguchi, S., Isaka, R., Sakahashi, Y., Tsujino, H., Haga, Y., Higashisaka, K., ... & Tsutsumi, Y. 2022. Silver nanoparticles suppress retinoic acid-induced neuronal differentiation in human-derived neuroblastoma sh-sy5y cells. ACS Applied Nano Materials, 5(12), 19025-19034. https://doi.org/10.1021/acsanm.2c04938.
- [15] Barth, M., Nienguesso, A. T., Santos, A. N., & Schmidt, C. 2022. Quantitative proteomics and in-cell cross-linking reveal cellular reorganisation during early neuronal differentiation of sh-sy5y cells. Communications Biology, 5(1). https://doi.org/10.1038/s42003-022-03478-7.

- [16] Jeon, S., Heo, J., Kim, M., Jeong, W., & Kang, H. 2020. High-precision 3d bio-dot printing to improve paracrine interaction between multiple types of cell spheroids. Advanced Functional Materials, 30(52). https://doi.org/10.1002/adfm.202005324
- [17] Gutzweiler, L., Kartmann, S., Troendle, K., Benning, L., Finkenzeller, G., Zengerle, R., ... & Zimmermann, S. 2017. Large scale production and controlled deposition of single huvec spheroids for bioprinting applications. Biofabrication, 9(2), 025027. https://doi.org/10.1088/1758-5090/aa7218.
- [18] Robu, A., Mironov, V., & Neagu, A. 2019. Using sacrificial cell spheroids for the bioprinting of perfusable 3d tissue and organ constructs: a computational study. Computational and Mathematical Methods in Medicine, 2019, 1-9. https://doi.org/10.1155/2019/7853586.
- [19] Zhao, L., Xiu, J., Liu, Y., Zhang, T., Pan, W., Zheng, X., ... & Zhang, X. 2019. A 3d printed hanging drop dripper for tumor spheroids analysis without recovery. Scientific Reports, 9(1). https://doi.org/10.1038/s41598-019-56241-0.
- [20] Suwannakot, P., Zhu, L., Tolentino, M., Du, E., Sexton, A., Myers, S., ... & Gooding, J. (2023). Electrostatically cross-linked bioinks for jetting-based bioprinting of 3d cell cultures. Acs Applied Bio Materials, 7(1), 269-283. https://doi.org/10.1021/acsabm.3c00849.
- [21] Benmeridja, L., Moor, L., Maere, E., Vanlauwe, F., Ryx, M., Tytgat, L., ... & Declercq, H. 2020. High-throughput fabrication of vascularized adipose microtissues for 3d bioprinting. Journal of Tissue Engineering and Regenerative Medicine, 14(6), 840-854. https://doi.org/10.1002/term.3051.
- [22] Moldovan, L., Barnard, A., Gil, C., Lin, Y., Grant, M., Yöder, M., ... & Moldovan, N. 2017. Ipsc-derived vascular cell spheroids as building blocks for scaffold-free biofabrication. Biotechnology Journal, 12(12). https://doi.org/10.1002/biot.201700444.
- [23] Jeon, O., Lee, Y., Hinton, T., Feinberg, A., & Alsberg, E. 2019. Cryopreserved cell-laden alginate microgel bioink for 3d bioprinting of living tissues. Materials Today Chemistry, 12, 61-70. https://doi.org/10.1016/j.mtchem.2018.11.009.
- [24] Decarli, M., Seijas-Gamardo, A., Morgan, F., Wieringa, P., Baker, M., Silva, J., ... & Mota, C. 2023. Bioprinting of stem cell spheroids followed by post-printing chondrogenic differentiation for cartilage tissue engineering. Advanced Healthcare Materials, 12(19). https://doi.org/10.1002/adhm.202203021.
- [25] Kim, J., Choi, Y., Gal, C., Sung, A., Park, H., & Yun, H. 2023. Development of an alginate–gelatin bioink enhancing osteogenic differentiation by gelatin release. International Journal of Bioprinting, 9(2), 660. https://doi.org/10.18063/ijb.v9i2.660.
- [26] Ayan, B., Zhang, Z., Celik, N., Zhou, K., Wu, Y., Costanzo, F., ... & Özbolat, İ. 2020. Aspiration-assisted freeform bioprinting of tissue spheroids in a yield-stress gel.. https://doi.org/10.1101/2020.05.31.122309.
- [27] Fayyazbakhsh, F., Khayat, M., & Leu, M. 2022. 3d-printed gelatin-alginate hydrogel dressings for burn wound healing: a comprehensive study. International Journal of Bioprinting, 8(4), 618. https://doi.org/10.18063/ijb.v8i4.618.
- [28] Erkoc, P., Uvak, I., Nazeer, M., Batool, S., Odeh, Y., Akdoğan, O., ... & Kızılel, S. 2020. 3d printing of cytocompatible gelatin-cellulose-alginate blend hydrogels. Macromolecular Bioscience, 20(10). https://doi.org/10.1002/mabi.202000106.
- [29] Zhu, Y., Stark, C., Madira, S., Ethiraj, S., Venkatesh, A., Anilkumar, S., ... & Woo, Y. 2022. Three-dimensional bioprinting with alginate by freeform reversible embedding of suspended hydrogels with tunable physical properties and cell proliferation. Bioengineering, 9(12), 807. https://doi.org/10.3390/bioengineering9120807.
- [30] Alruwaili, M., López, J., McCarthy, K., Reynaud, E., & Rodriguez, B. 2019. Liquid-phase 3d bioprinting of gelatin alginate hydrogels: influence of printing parameters on hydrogel line width and layer height. Bio-Design and Manufacturing, 2(3), 172-180. https://doi.org/10.1007/s42242-019-00043-w.
- [31] Lee, J., Park, D., Yang, L., Kim, E., Ahrberg, C., Lee, K., ... & Chung, B. 2018. Generation of uniform-sized multicellular tumor spheroids using hydrogel microwells for advanced drug screening. Scientific Reports, 8(1). https://doi.org/10.1038/s41598-018-35216-7.
- [32] Huang, G., Tseng, C., Yen, B., Dai, L., Hsieh, P., & Hsu, S. 2013. Solid freeform-fabricated scaffolds designed to carry multicellular mesenchymal stem cell spheroids for cartilage regeneration. eCM, 26, 179-194. https://doi.org/10.22203/ecm.v026a13.

- [33] Krishnan, M. and Chelvam, V. 2021. Developing μsphereplatform using a commercial hairbrush: an agarose 3d culture platform for deep-tissue imaging of prostate cancer. Acs Applied Bio Materials, 4(5), 4254-4270. https://doi.org/10.1021/acsabm.1c00086.
- [34] Desai, P., Tseng, H., & Souza, G. 2017. Assembly of hepatocyte spheroids using magnetic 3d cell culture for cyp450 inhibition/induction. International Journal of Molecular Sciences, 18(5), 1085. https://doi.org/10.3390/ijms18051085.
- [35] Sogomonyan, A., Shipunova, V., Soloviev, V., Larionov, V., Kotelnikova, P., & Deyev, S. 2022. 3d models of cellular spheroids as a universal tool for studying the cytotoxic properties of anticancer compounds in vitro. Acta Naturae, 14(1), 92-100. https://doi.org/10.32607/actanaturae.11603.
- [36] Liu, G., Thangavel, R., Rysted, J., Kim, Y., Francis, M., Adams, E., ... & Lee, G. 2019. Loss of tau and fyn reduces compensatory effects of map2 for tau and reveals a fyn-independent effect of tau on calcium. Journal of Neuroscience Research, 97(11), 1393-1413. https://doi.org/10.1002/jnr.24517.
- [37] Li, Q., Zhang, W., Qiao, X., Liu, C., Dao, J., Qiao, C., ... & Zhao, W. 2023. Reducing polypyrimidine tract-binding protein 1 fails to promote neuronal transdifferentiation on ht22 and mouse astrocyte cells under physiological conditions. Experimental and Therapeutic Medicine, 27(2). https://doi.org/10.3892/etm.2023.12360.
- [38] Ko, K., Tam, N., Teixeira, A., & Frampton, J. 2019. Sh-sy5y and luhmes cells display differential sensitivity to mpp+, tunicamycin, and epoxomicin in 2d and 3d cell culture. Biotechnology Progress, 36(2). https://doi.org/10.1002/btpr.2942.
- [39] Onbas, R. and Yıldız, A. 2021. Fabrication of tunable 3d cellular structures in high volume using magnetic levitation guided assembly. Acs Applied Bio Materials, 4(2), 1794-1802. https://doi.org/10.1021/acsabm.0c01523.
- [40] Xu, Z., Yang, D., Huang, X., & Huang, H. 2021. Astragaloside iv protects 6-hydroxydopamine-induced sh-sy5y cell model of parkinson's disease via activating the jak2/stat3 pathway. Frontiers in Neuroscience, 15. https://doi.org/10.3389/fnins.2021.631501.